RESEARCH ARTICLE

Intrinsic Kinematics of the Tibiotalar and Subtalar Joints during Human Walking based on Dynamic Biplanar Fluoroscopy

Shengli Wang[1] · Zhihui Qian[1] · Xiangyu Liu[1] · Guangsheng Song[1] · Kunyang Wang[1] · Jianan Wu[1] · Jing Liu[1] · Lei Ren[1,2] · Luquan Ren[1]

Abstract

Accurate knowledge of the kinematics of the in vivo Ankle Joint Complex (AJC) is critical for understanding the biomechanical function of the foot and assessing postoperative rehabilitation of ankle disorders, as well as an essential guide to the design of ankle–foot assistant devices. However, detailed analysis of the continuous 3D motion of the tibiotalar and subtalar joints during normal walking throughout the stance phase is still considered to be lacking. In this study, dynamic radiographs of the hindfoot were acquired from eight subjects during normal walking. Natural motions with six Degrees of Freedom (DOF) and the coupled patterns of the two joints were analyzed. It was found that the movements of the two joints were mostly in opposite directions (including rotation and translation), mainly in the early and late stages. There were significant differences in the Range of Motion (ROM) in Dorsiflexion/Plantarflexion (D/P), Inversion/Eversion (In/Ev), and Anterior–Posterior (AP) and Medial–Lateral (ML) translation of the tibiotalar and subtalar joints ($p < 0.05$). Plantarflexion of the tibiotalar joint was coupled with eversion and posterior translation of the subtalar joint during the impact phase ($R^2 = 0.87$ and 0.86, respectively), and plantarflexion of the tibiotalar joint was coupled with inversion and anterior translation of the subtalar joint during the push-off phase ($R^2 = 0.93$ and 0.75, respectively). This coordinated coupled motion of the two joints may be a manifestation of the AJC to move flexibly while bearing weight and still have stability.

Keywords Dynamic biplane radiography · Tibiotalar joint · Subtalar joint · In vivo kinematics · Coupled motion · Bionic design

1 Introduction

The Ankle Joint Complex (AJC) is generally subjected to a large mechanical load (impact force) at the moment of touchdown and subsequently transfers ground reaction forces to the leg to propel the body forward [1–4]. This requires the AJC to have flexible motion modulation and the ability to maintain joint stability [5], and for the AJC to achieve this dual role, it may heavily rely on the coordinated motion of the tibiotalar and subtalar joints. A thorough understanding of the Three-Dimensional (3D) motion of these two joints in the hindfoot can guide the diagnosis of ankle-related injuries and disorders, as well as for the design of prostheses, orthotics, and bionic robotic feet [6].

During the past decades, numerous studies have been conducted on AJC kinematics. Among them, Optical Motion Capture (OMC) techniques and multisegmental foot models have been widely used in related research [7–13]; however, accurate measurement of the 3D motion of the tibiotalar and subtalar using the OMC is difficult to achieve because of the difficulty in placing the corresponding landmarks of the hindfoot [14, 15]. In particular, the talus is surrounded by ligaments and muscles and lacks external markers, making it difficult to accurately measure its movement with skin markers. To overcome the limitations of skin markers, bone pins with reflex markers have been imbedded in foot bones to capture individual bones during in vivo joint motion [16–20]. This method of measuring foot and ankle kinematics is reproducible

✉ Zhihui Qian
zhqian@jlu.edu.cn

✉ Lei Ren
lei.ren@manchester.ac.uk

[1] Key Laboratory of Bionic Engineering, Jilin University, Changchun 130022, China

[2] School of Mechanical, Aerospace and Civil Engineering, University of Manchester, Manchester M13 9PL, UK

between subjects [20]. However, this approach is invasive and requires local anesthesia and surgery on the subject, and related studies have involved a smaller number of subjects. Recently, dynamic radiographic imaging systems were employed to analyze the spatial motion of AJC under different conditions. Single-plane radiographic systems (e.g., C-arm) have been widely used to capture joint motion [21–25], and since it has only one X-ray transmitter and one receiver, the images obtained from one direction. Therefore, its limitation in quantifying the out-of-plane Degrees of Freedom (DOF) restricts a more comprehensive quantification of the in vivo realistic motion of the target joints.

Biplanar dynamic fluoroscopy systems combined with model-based 2D-3D registration technology are relatively advanced devices and methods to reveal the spatial motion of target joints [26–34], mostly for kinematic studies of ankle disorders or injuries. For the intrinsic kinematic studies of the tibiotalar and subtalar in healthy subjects with normal gait, de Asla et al. recorded three positions in quasi-static conditions using a dual-orthogonal fluoroscopic system [35]. Furthermore, one study quantified three rotational movements of the ankle using a dynamic biplanar fluoroscopy system [36]. Roach et al. analyzed the 3D kinematics of the two joints during the heel-strike and toe-off phases, respectively [37]. Those studies deepen the understanding of the kinematics of the joint kinematics of the hindfoot. However, the detailed description of continuous 3D motion (including rotation and translation) during normal walking throughout the stance phase of gait is still considered to be lacking. Moreover, the kinematic coupling of these two joints and their biomechanical functions need further exploration.

This study aims to provide continuous rotational and translational kinematic waveforms, as well as Range of Motions (ROMs) of six DOF, to further reveal the six DOF kinematic coupling relationship between the tibiotalar and subtalar, including the relationship between the rotational motions of the two joints and the relationship between rotation and translation. Further analysis of the biomechanical functions (joint stability and flexibility) corresponding to the primary movements with coupled relationships was also discussed.

2 Materials and methods

Eight healthy adult subjects (age 26.3 ± 1.0 years; height 175.6 ± 4.4 cm; weight 74.1 ± 5.9 kg) with no experience of ankle disease or injury participated in this study, and each was given a description of the experimental project to be completed. The Ethics Committee at The Second Hospital of Jilin University approved this project (No. 2020085).

2.1 Data collection

A 5.6 m long walkway was provided for subjects to walk on, and a 50 mm thick high-density polystyrene foam board was laid on top of the walkway to reduce the occlusion of the plantar by the plane of the walkway in the radiographs [36, 38]. The subjects walked on the indoor walkway at their own controlled natural pace, making sure their right foot landed on the collection area each time after several exercises. The dynamic biplanar fluoroscopy system (Imaging Systems & Service Inc., USA) (Fig. 1a) worked at 100 Hz to acquire radiographs. A lead suit was prepared for participants for protection. The operating parameters of the X-ray tubes were 55 kV and 80 mA, with a high-speed camera exposure time of 1 ms. The radiograph sequences (Fig. 1c) of the subject's right foot were acquired from heel strike to toe-off (Fig. 1b), ensuring that 4 or 5 complete image sequences were acquired for each subject.

2.2 CT scans and definition of anatomical coordinate system

Volume image data of the target joints were collected using a Computed Tomography (CT) scanner (Brilliance iCT 256, Philips, Netherlands), and the parameters were as follows: thickness, 0.8 mm; image matrix, 512×512 pixels. Image segmentation and model reconstruction were then performed using OsiriX software (Pixmeo, Geneva, Switzerland) to obtain 3D volumes and polygonal mesh models for the tibia, talus, and calcaneus [39–41]. The 3D volumes were used for model-based tracking and registration, and the polygonal mesh models were then used to establish the Anatomical Coordinate System (ACS).

The ACS was defined for each bone based on a combination of geometry and anatomical landmarks (Fig. 2) using Geomagic software (Geomagic Wrap, USA) according to previously published methods [22, 42–44].

2.3 Data processing

Images obtained with a dynamic biplanar fluoroscopy system were inevitably distorted due to the conversion of X-ray to grayscale images involved. All radiographs of the target joint were undistorted using "standard grid" images and the distortion-correcting algorithm in XMALab software (XMALab, Brown University, USA). In addition, a Lego-based calibration cube (with known geometry) was used to calibrate the 3D space in order to get data for reconstructing the virtual 3D environment [45, 46].
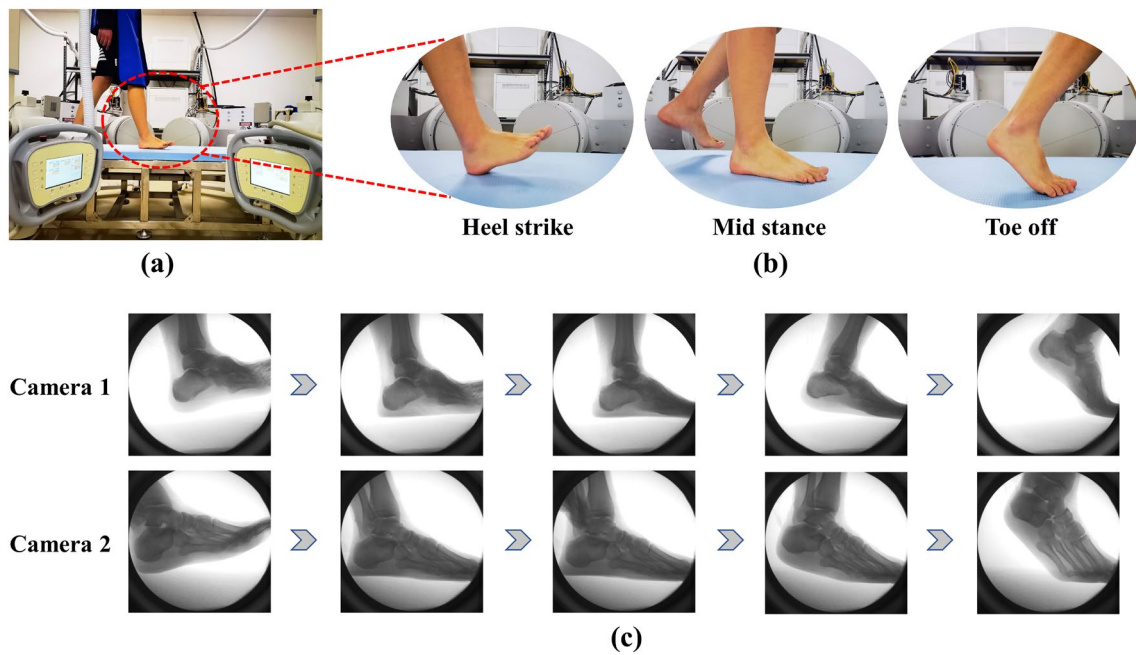
Heel strike   **Mid stance**   **Toe off**

(a)   **(b)**

Camera 1

Camera 2

(c)

Fig. 1 **a** Ankle motion capture by the dynamic biplanar fluoroscopy system. **b** Three special states of the foot during stance phase of gait. **c** The radiograph sequences from camera 1 and camera 2
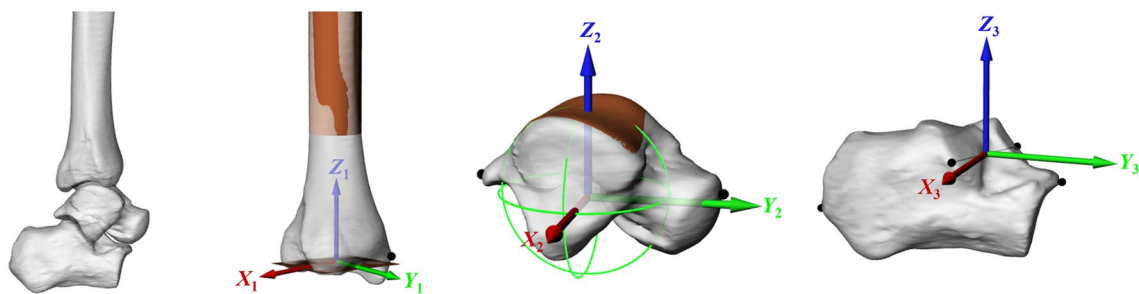

Fig. 2 An anatomical coordinate system was created for each bone using a combination of geometric shapes and anatomical landmarks

Autoscoper software (Autoscoper V2, Brown University, USA) was used to perform model-based tracking in a virtual 3D environment to reproduce the realistic motion of the target skeleton [47–50]. Model-based tracking consists of three main steps: creating Digitally Reconstructed Radiographs (DRRs) in the virtual 3D environment, then manually completing the initial frame alignment, and finally executing an optimization algorithm to track automatically. When each bone is simultaneously registered to the images of both cameras, an automatic registration algorithm is executed for all frames (Fig. 3), the 4×4 transformation matrix corresponding to the DRRs in the 3D environment is then obtained.

2.4 Statistical analysis

The ACSs as shown in Fig. 2 were used for the analysis of 6 DOF motion of joints. X-axis was in the Medial–Lateral (ML) direction, along which direction ML translation was reported and around which Dorsiflexion/Plantarflexion (D/P) occurs. The Y-axis was in the Anterior–Posterior (AP) direction, along which AP translation was reported and around which Inversion/Eversion (In/Ev) occurs; the Z-axis was in the Proximal–Distal (PD) direction, along which PD translation was reported and around which Adduction/Abduction (Ad/Ab) occurs. Joint angles and translations were described as relative motion of the distal bone relative to the proximal
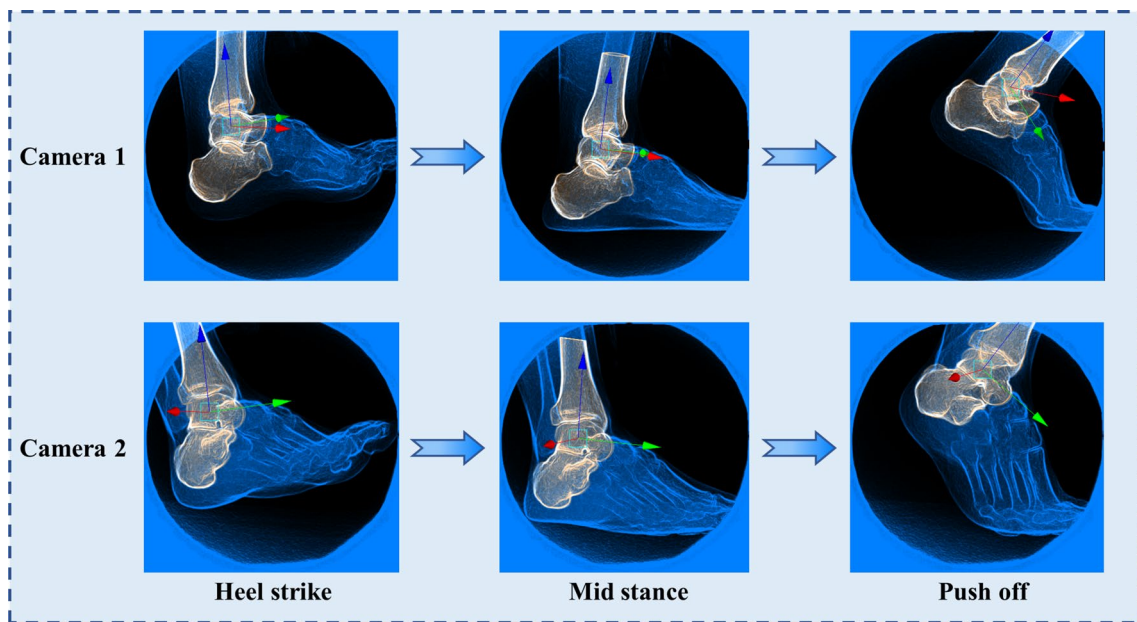
Fig. 3 Model-based tracking reproduced the 3D pose of each bone. The illustration shows the registration status of bone models of the tibiotalar and subtalar joints with biplanar radiography at three moments: heel strike, mid-stance and push off (See Supplementary Material 1 for a video)
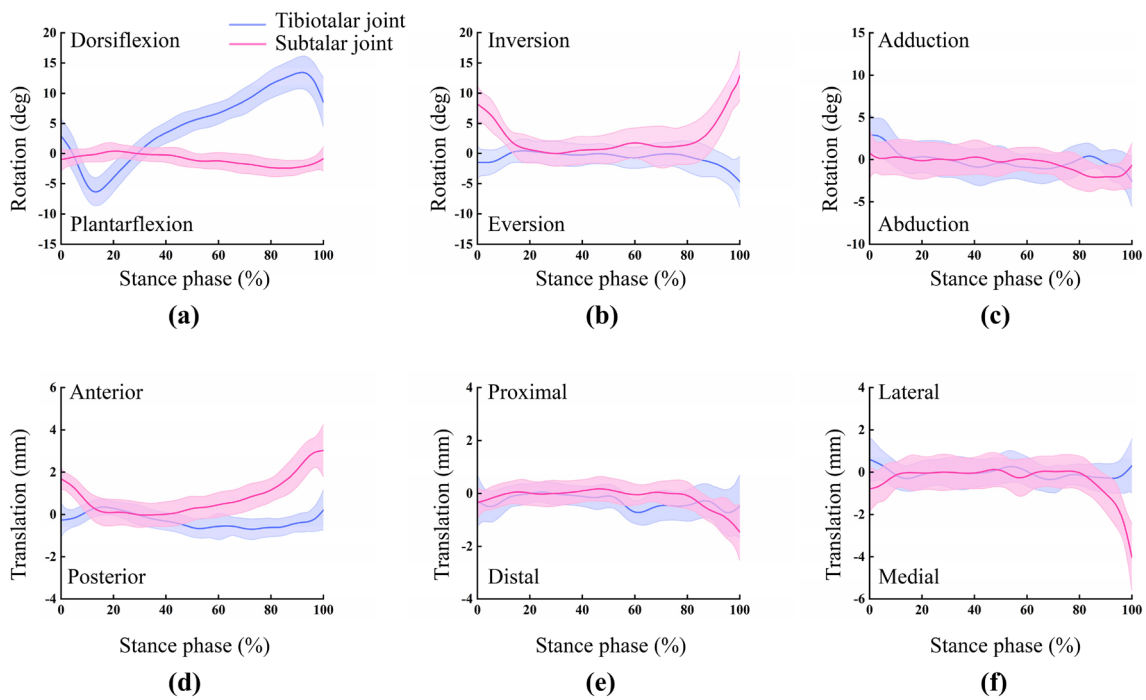

Fig. 4 Continuous kinematic waveforms of the tibiotalar and subtalar joints. The top row represents three rotations, and the bottom row represents three translations. The values of 0% and 100% of the horizontal axes correspond to heel strike and toe off, respectively. Shaded regions indicate ± 1 standard deviation

bone. Kinematics data were calculated by the transformation matrix and correlating it with the ACSs [51]. The data of each trial for each subject were normalized to 100% stage.

The phase before maximum plantarflexion and the phase after maximum dorsiflexion were used to define the impact phase and push-off phases for the coupled motion analysis [15]. The R^2 and the slope of the fitted curve indicated the degree of coupling.

3 Results

3.1 Dynamic Continuous Kinematics

The continuous kinematic waveforms of the tibiotalar and subtalar joints of the eight subjects are shown in Fig. 4, demonstrating the mean dynamic rotational angles and relative translations with gait percentage. Obviously, the significant changes in motion at each DOF occurred mainly at the beginning and end of the phase, except for the D/P of the tibiotalar joint, and the waveform was relatively flat during the middle phase. Apparently, in the three rotational DOFs, the two joints move in exactly the opposite direction (mainly occurring the early stage and late stage of the stance phase). For joint translation, the opposite direction of motion was also found, which were mainly manifested in the AP and ML directions during the early stage and in the ML direction during the late stage.

3.2 Range of Motion

As shown in Fig. 5a, a bar chart comparing the ROM of the two joints at six DOF. The D/P and In/Ev ROMs of the two joints were significantly different ($P < 0.001$ and $P < 0.01$, respectively). For rotational DOF, D/P of the tibiotalar joint was more pronounced, while the subtalar joint mainly exhibited In/Ev. For Ad/Ab, the difference in ROM between the

two joints was small ($P = 0.15$), and the waveform was relatively gentle (Fig. 4c). As shown in Fig. 5b, for translational movements, the ROM was significantly larger in the AP and ML directions for the subtalar joint ($P < 0.05$ and $P < 0.001$, respectively). In addition, for translations in the PD direction, there was a small difference in ROM between the two joints ($P = 0.49$).

3.3 Coupled Motion between Two Joints

As shown in Fig. 6, plantarflexion of the tibiotalar joint was coupled with eversion of the subtalar joint during the impact phase (average slope: − 1.29, indicating that for every 1° of plantarflexion of the tibiotalar joint, the subtalar joint eversion was 1.29°; average $R^2 = 0.87$) (Fig. 6a). During the push-off phase, plantarflexion of the tibiotalar was coupled with inversion of the subtalar joint (average slope: 2.05, indicating that for every 1° of plantarflexion of the tibiotalar joint, the subtalar joint inversion was 2.05°; average $R^2 = 0.93$) (Fig. 6b). In addition, the plantarflexion of the tibiotalar joint was coupled with the posterior translation of the subtalar joint during the impact phase (average slope: − 0.21, indicating that for every 1° of plantarflexion of the tibiotalar joint, the posterior translation of the subtalar was 0.21 mm; average $R^2 = 0.86$) (Fig. 6c). The plantarflexion of the tibiotalar joint was coupled with the anterior translation of the subtalar during the push-off phase (average slope: 0.18, indicating that for every 1° of plantarflexion of the tibiotalar joint, the anterior translation of the subtalar was 0.18 mm; average $R^2 = 0.75$) (Fig. 6d).

4 Discussion

In this study, a dynamic biplanar fluoroscopy system combined with semiautomatic 2D-3D registration technology was used to measure the complex and subtle 3D kinematics
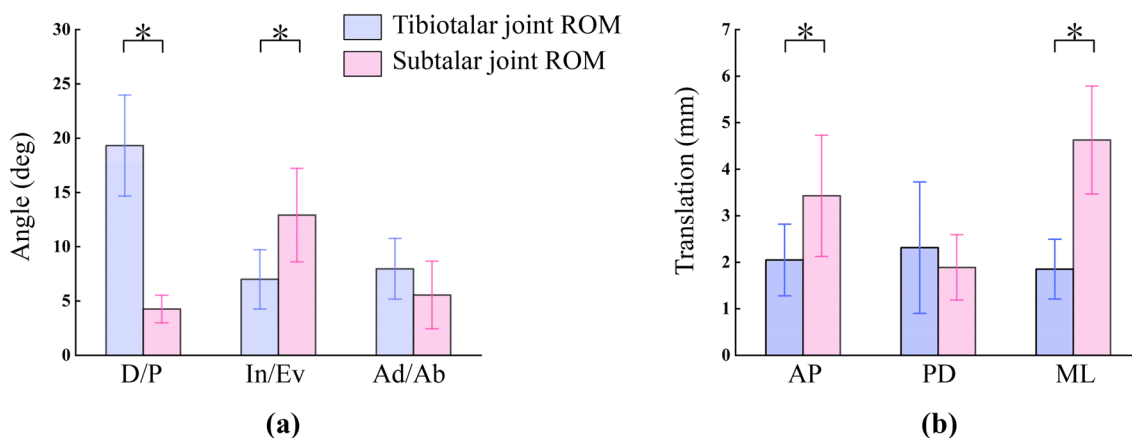

Fig. 5 Rotational and translational ROM of the tibiotalar and subtalar joints, data are displayed as mean ± standard deviation, *p < 0.05
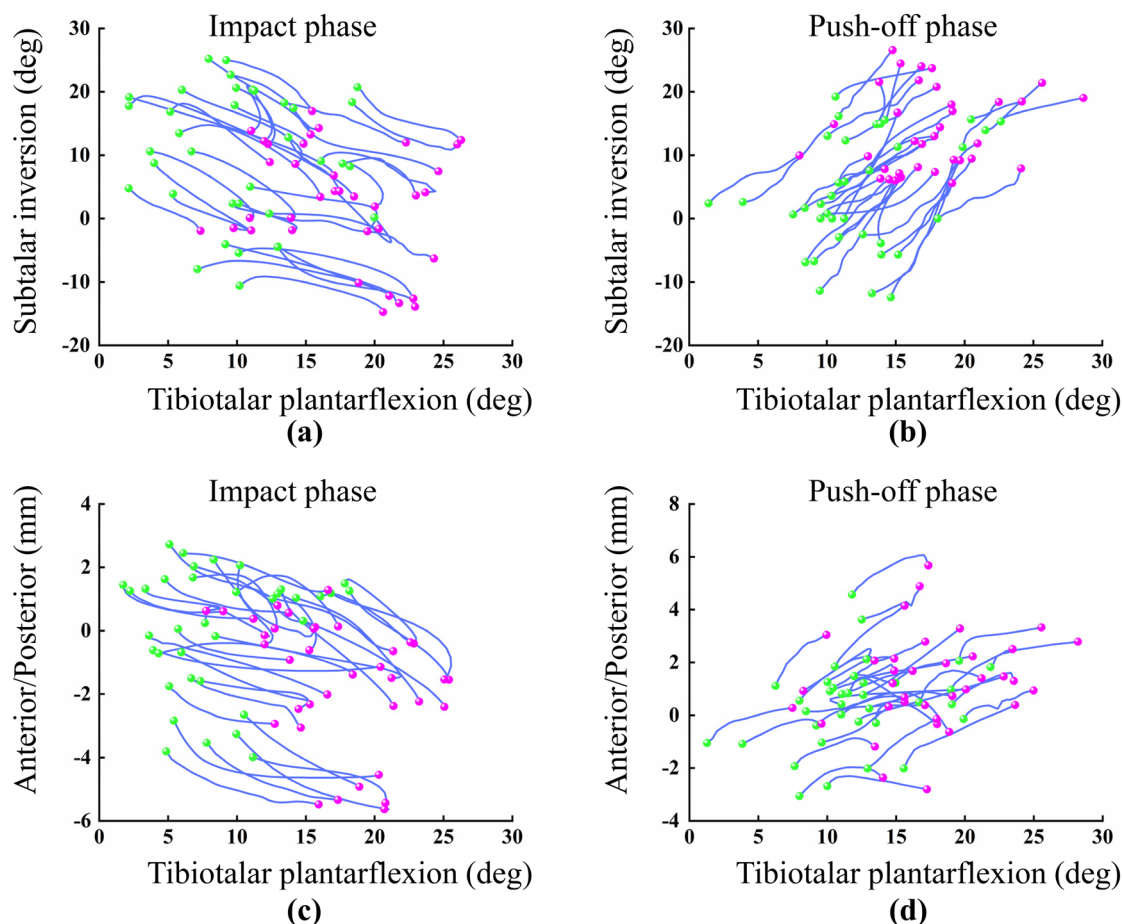
Fig. 6 Coupled motion representation of the tibiotalar and subtalar joints during the impact phase and push-off phase. The green and red dots represent the beginning and end of the corresponding phase

Table 1 ROMs data were compared in this study with those of previous studies, and these studies all used the biplanar fluoroscopy system

	Current study		Koo et al		Roach et al		Yang et al		Peltz et al	
	Tibiotalar	Subtalar	Tibiotalar	Subtalar	Tibiotalar	Subtalar	Tibiotalar	Subtalar	Tibiotalar	Subtalar
D/P (°)	19.3±4.6	4.3±1.2	18.5±3.5	6.6±2.8	16.3(13.1,19.5)	8.6(6.1,11.1)	12.3±2.8	2.4±0.6	28.2±8.3	3.6±1.7
In/Ev (°)	7.0±2.7	12.9±4.3	5.1±1.1	6.6±4.5	3.8(2.5,5.1)	11.3(9.5,13.1)	3.8±1.7	9.4±2.9	2.9±1.2	7.4±3.4
Ad/Ab (°)	7.9±2.8	5.6±3.1	8.6±3.9	5.6±2.7	7.4(4.4,10.1)	12.5(9.8,15.2)	5.9±2.3	2.8±1.3	7.0±1.4	4.5±1.8
AP (mm)	2.0±0.7	3.4±1.3	–	–	–	–	4.5±1.2	1.9±0.5	–	–
ML (mm)	1.8±0.6	4.6±1.2	–	–	–	–	2.2±0.6	2.3±0.6	–	–
PD (mm)	2.3±1.4	1.8±0.7	–	–	–	–	1.2±0.6	1.7±0.4	–	–

Parentheses indicate 95% confidence intervals. Data presented as the mean ± standard deviation unless otherwise noted [15, 36, 37, 52]

of the hindfoot joints of healthy adult male subjects. This includes dynamic continuous motion, ROMs and the association of motion of two joints in different directions. Relative to the other two directions of rotational motion, the tibiotalar was mainly responsible for D/P, while the subtalar was mainly responsible for In/Ev (Fig. 4 and Table 1), which was consistent with previous studies [15, 36, 37].

Dynamic continuous kinematics waveform shows that the two joints tend to exhibit opposite trends, including rotation and translation. The opposite trend of the motion of the two joints may be an important way to regulate joint movement, to support weight-bearing, motion and stability of the foot. The two joints exhibit a range of fluctuations in Ad/Ab, which may come to accommodate variable load
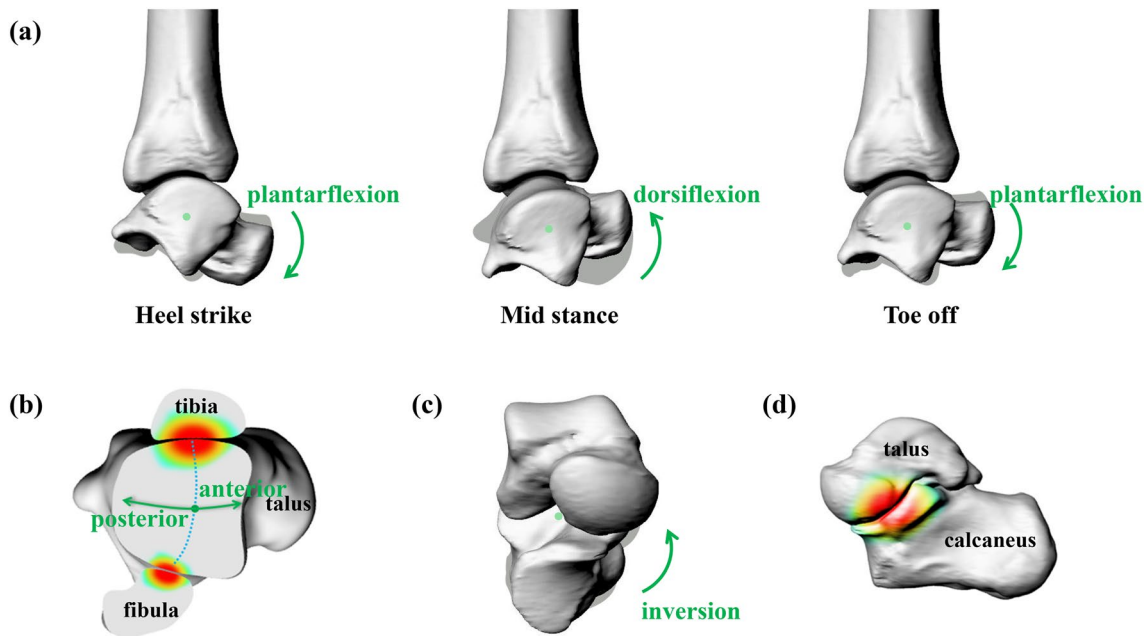
Fig. 7 Diagram of the relative motion of the joints, with arrows indicating the direction of motion (rotation or translation). The gradient ramp indicates the degree of closeness of the articular surface. **a** Lateral view of the tibiotalar joint; **b** Top view of the talocrural joint (transverse plane); **c** Anterior view of the subtalar joint; **d** Medial view of the subtalar joint

distribution and contribute to overall ankle stability and gait stability. Some conclusions of this study are similar to those of Roach et al., but there are also essential differences [37]. They reported that only radiographs of heel strike and toe-off periods were captured on a treadmill at the speed of 0.5 m/s and 1.0 m/s, and the kinematic analysis was made, with discontinuous gait. In this study, continuous motion was captured throughout the stance phase at a natural pace chosen by the subject.

During the 15–90% phase, the tibiotalar joint changed dorsiflexion (Fig. 4a), with a slight posterior translation of the talus relative to the tibia (Fig. 4d). The cross section of the talus is wide at the front and narrow at the back, while the entire ankle joint is mortise and tenon construction (Fig. 7a, b), which makes the articular surface closer, and the tibiotalar joint becomes increasingly stable. The mortise structure limits the ML translation of the talus, which minimizes the ML ROM of the tibiotalar joint, as shown in Fig. 5b and Table 1. The joint motion is accompanied by a change in the contact pattern of the joint surface, which allows the talocrural joint to exhibit better stability. During the early stage and late stage, plantarflexion of the talus is accompanied by anterior translation (Fig. 4a, d), the posterior end of the talus with a narrower cross-section slides into the mortise (Fig. 7a, b), and the joint becomes lax and more flexible. Therefore, it can quickly adapt to the impact force during the early stage and prepare for the swing during the late stage.

The subtalar joint was almost in an inversion state during the entire phase (Fig. 4b). The calcaneus inversion with respect to the talus will cause the two bones to join more closely at the mid-articular surface of the calcaneus (Fig. 7c, d), which will make the subtalar joint more stable. As a result, the articular surface contact pattern of the two joints changes (perhaps accompanied by ligament tensioning or relaxation), causing the tibiotalar and subtalar joints to appear flexible or stable at a particular stage.

From Table 1, it is evident that the ROMs we provided have some similarities with the results of the four previous studies [15, 36, 37, 52]. The ROMs given by different studies have some variability, as does the kinematic waveform, which is related to the principle of establishing the coordinate system and the mathematical calculation method. In addition, it is also related to the subject's sex and age and the test conditions. For example, the D/P ROM reported by Peltz et al. was significantly larger at $28.2 \pm 8.3°$, which may be related to the test being performed under running conditions. Again, Roach et al. collected heel strike and push-off phases from subjects without a mid-stance phase, leading to some discrepancies between the results of that study and ours.

In addition, we provide translational ROMs in three directions that differ somewhat from the translational ROMs reported by Yang et al. (Table 1). Our results show the smallest ML translation of the tibiotalar joint and the largest PD translation. This may be related to the fact that the mortise

structure of the talocrural joint restricts the translation of the talus in the ML direction, while the joint gaps in the PD direction provide a cushioning effect when there is a touchdown impact. In contrast, there is less PD translation and more ML translation of the subtalar joint. This may be because the tight joint surface has little clearance in the PD direction and less restriction in the ML direction. Therefore, the translation ROMs provided by this study may be more reasonable.

There was a clear coupling relationship between the dominant movement of the two joints, and this phenomenon occurs mainly at the impact and push-off phase. The synergistic relationship between the rotational DOF of the two joints has been mentioned by Yang et al. [15]. In addition, we also found that there was a clear coupling relationship between the rotation and the translation of the two joints; that is, the plantarflexion of the tibiotalar was coupled with posterior and anterior translation of the subtalar during the impact and push-off phase, respectively. Revealing the coupled motion relationship between joints is a step forward for our understanding of the 3D intrinsic kinematics of the AJC.

There are still some limitations of the study. First, the imaging area of dynamic biplanar fluoroscopy system is limited, and the distal tibia is out of view at the end of the toe off. Thus, the last few frames at push-off are ignored, which is a common problem of studying the hindfoot kinematics using the dynamic biplanar fluoroscopy system [37, 49, 50]. Second, this study only involved male subjects, and possible sex differences in hindfoot joint kinematics should be considered in further work. Future studies can also focus on more special motion patterns, such as running at different speeds, vertical jumping, and lateral jumping, because special activities may show foot joint functions more clearly.

5 Conclusion

In conclusion, the results of this study showed that the rotation and translation of the two joints were in opposite directions during the early stage and late stage of the stance phase. Moreover, there was a significant coupling between plantarflexion of the tibiotalar joint and the In/Ev and AP movement of the subtalar joint during the impact phase and push-off phase. The shape of the joint surfaces and the ROM in the specified directions have a synergistic effect on the stiffness adjustment of the joints, giving stability and flexibility to both joints in particular phases. This offers a more comprehensive and precise understanding of the 3D motion of the two joints, which may provide a detailed reference for the assessment of postoperative ankle motion rehabilitation and the design of ankle–foot assistant devices.

Data availability Data and explanations related to this study are available upon reasonable request by contacting the corresponding author.

Declarations

Conflict of interest The authors declare that they have no competing interests.

References

1. Boonpratatong, A., & Ren, L. (2010). The human ankle-foot complex as a multi-configurable mechanism during the stance phase of walking. *Journal of Bionic Engineering, 7*, 211–218.
2. Jastifer, J. R., & Gustafson, P. A. (2014). The subtalar joint: biomechanics and functional representations in the literature. *The Foot, 24*, 203–209.
3. Krähenbühl, N., Horn-Lang, T., Hintermann, B., & Knupp, M. (2017). The subtalar joint: a complex mechanism. *EFORT Open Reviews, 2*, 309–316.
4. Sarrafian, S. K. (1993). Biomechanics of the subtalar joint complex. *Clinical Orthopaedics and Related Research, 290*, 17–26.
5. Mckeon, J. M. M., & Hoch, M. C. (2019). The ankle-joint complex: a kinesiologic approach to lateral ankle sprains. *Journal of Athletic Training, 54*, 589–602.
6. Wang, K. Y., Ren, L., Qian, Z. H., Liu, J., Geng, T., & Ren, L. Q. (2021). Development of a 3d printed bipedal robot: towards humanoid research platform to study human musculoskeletal biomechanics. *Journal of Bionic Engineering, 18*, 150–170.
7. Reinschmidt, C., Van Den Bogert, A., Murphy, N., Lundberg, A., & Nigg, B. (1997). Tibiocalcaneal motion during running, measured with external and bone markers. *Clinical Biomechanics, 12*, 8–16.
8. Carson, M. C., Harrington, M. E., Thompson, N., O'connor, J. J., & Theologis, T. N. (2001). Kinematic analysis of a multi-segment foot model for research and clinical applications: a repeatability analysis. *Journal of Biomechanics, 34*, 1299–1307.
9. Stebbins, J., Harrington, M., Thompson, N., Zavatsky, A., & Theologis, T. (2006). Repeatability of a model for measuring multi-segment foot kinematics in children. *Gait & Posture, 23*, 401–410.
10. Jenkyn, T. R., & Nicol, A. C. (2007). A multi-segment kinematic model of the foot with a novel definition of forefoot motion for use

in clinical gait analysis during walking. *Journal of Biomechanics, 40*, 3271–3278.

11. Bruening, D. A., Cooney, K. M., & Buczek, F. L. (2012). Analysis of a kinetic multi-segment foot model. Part i: Model repeatability and kinematic validity. *Gait & Posture, 35*, 529–534.

12. Kelly, L. A., Cresswell, A. G., Racinais, S., Whiteley, R., & Lichtwark, G. (2014). Intrinsic foot muscles have the capacity to control deformation of the longitudinal arch. *Journal of The Royal Society Interface, 11*, 20131188.

13. Sekiguchi, Y., Kokubun, T., Hanawa, H., Shono, H., Tsuruta, A., & Kanemura, N. (2020). Evaluation of the validity, reliability, and kinematic characteristics of multi-segment foot models in motion capture. *Sensors, 20*, 4415.

14. Pitcairn, S., Kromka, J., Hogan, M., & Anderst, W. (2020). Validation and application of dynamic biplane radiography to study in vivo ankle joint kinematics during high-demand activities. *Journal of Biomechanics, 103*, 109696.

15. Yang, S., Canton, S. P., Hogan, M. V., & Anderst, W. (2021). Healthy ankle and hindfoot kinematics during gait: Sex differences, asymmetry and coupled motion revealed through dynamic biplane radiography. *Journal of Biomechanics, 116*, 110220.

16. Westblad, P., Hashimoto, T., Winson, I., Lundberg, A., & Arndt, A. (2002). Differences in ankle-joint complex motion during the stance phase of walking as measured by superficial and bone-anchored markers. *Foot & Ankle International, 23*, 856–863.

17. Arndt, A., Westblad, P., Winson, I., Hashimoto, T., & Lundberg, A. (2004). Ankle and subtalar kinematics measured with intracortical pins during the stance phase of walking. *Foot & Ankle International, 25*, 357–364.

18. Arndt, A., Wolf, P., Liu, A., Nester, C., Stacoff, A., Jones, R., Lundgren, P., & Lundberg, A. (2007). Intrinsic foot kinematics measured in vivo during the stance phase of slow running. *Journal of Biomechanics, 40*, 2672–2678.

19. Nester, C., Jones, R. K., Liu, A., Howard, D., Lundberg, A., Arndt, A., Lundgren, P., Stacoff, A., & Wolf, P. (2007). Foot kinematics during walking measured using bone and surface mounted markers. *Journal of Biomechanics, 40*, 3412–3423.

20. Lundgren, P., Nester, C., Liu, A., Arndt, A., Jones, R., Stacoff, A., Wolf, P., & Lundberg, A. (2008). Invasive in vivo measurement of rear-, mid-and forefoot motion during walking. *Gait & Posture, 28*, 93–100.

21. Komistek, R. D., Stiehl, J. B., Buechel, F. F., Northcut, E. J., & Hajner, M. E. (2000). A determination of ankle kinematics using fluoroscopy. *Foot & Ankle International, 21*, 343–350.

22. Yamaguchi, S., Sasho, T., Kato, H., Kuroyanagi, Y., & Banks, S. A. (2009). Ankle and subtalar kinematics during dorsiflexion-plantarflexion activities. *Foot & Ankle International, 30*, 361–366.

23. Fukano, M., Kuroyanagi, Y., Fukubayashi, T., & Banks, S. (2014). Three-dimensional kinematics of the talocrural and subtalar joints during drop landing. *Journal of Applied Biomechanics, 30*, 160–165.

24. Mchenry, B. D., Exten, E. L., Long, J., Law, B., Marks, R. M., & Harris, G. (2015). Sagittal subtalar and talocrural joint assessment with weight-bearing fluoroscopy during barefoot ambulation. *Foot & Ankle International, 36*, 430–435.

25. Mchenry, B. D., Exten, E. L., Cross, J. A., Kruger, K. M., Law, B., Fritz, J. M., & Harris, G. (2017). Sagittal subtalar and talocrural joint assessment during ambulation with controlled ankle movement (cam) boots. *Foot & Ankle International, 38*, 1260–1266.

26. Kozanek, M., Rubash, H. E., Li, G., & De Asla, R. J. (2009). Effect of post-traumatic tibiotalar osteoarthritis on kinematics of the ankle joint complex. *Foot & Ankle International, 30*, 734–740.

27. Wainright, W. B., Spritzer, C. E., Lee, J. Y., Easley, M. E., Deorio, J. K., Nunley, J. A., & Defrate, L. E. (2012). The effect of modified broström-gould repair for lateral ankle instability on in vivo

tibiotalar kinematics. *The American Journal of Sports Medicine, 40*, 2099–2104.

28. Nichols, J. A., Roach, K. E., Fiorentino, N. M., & Anderson, A. E. (2016). Predicting tibiotalar and subtalar joint angles from skin-marker data with dual-fluoroscopy as a reference standard. *Gait & Posture, 49*, 136–143.

29. Nichols, J. A., Roach, K. E., Fiorentino, N. M., & Anderson, A. E. (2017). Subject-specific axes of rotation based on talar morphology do not improve predictions of tibiotalar and subtalar joint kinematics. *Annals of Biomedical Engineering, 45*, 2109–2121.

30. Roach, K. E., Foreman, K. B., Barg, A., Saltzman, C. L., & Anderson, A. E. (2017). Application of high-speed dual fluoroscopy to study in vivo tibiotalar and subtalar kinematics in patients with chronic ankle instability and asymptomatic control subjects during dynamic activities. *Foot & Ankle International, 38*, 1236–1248.

31. Lin, C. C., Li, J. D., Lu, T. W., Kuo, M. Y., Kuo, C. C., & Hsu, H. C. (2018). A model-based tracking method for measuring 3d dynamic joint motion using an alternating biplane x-ray imaging system. *Medical Physics, 45*, 3637–3649.

32. Cao, S. X., Wang, C., Ma, X., Wang, X., Huang, J. Z., Zhang, C., Chen, L., Geng, X., & Wang, K. (2019). In vivo kinematics of functional ankle instability patients and lateral ankle sprain copers during stair descent. *Journal of Orthopaedic Research, 37*, 1860–1867.

33. Cao, S. X., Wang, C., Zhang, G. H., Ma, X., Wang, X., Huang, J. Z., Zhang, C., & Wang, K. (2019). In vivo kinematics of functional ankle instability patients during the stance phase of walking. *Gait & Posture, 73*, 262–268.

34. Roach, K. E., Foreman, K. B., Macwilliams, B. A., Karpos, K., Nichols, J., & Anderson, A. E. (2021). The modified shriners hospitals for children greenville (mshcg) multi-segment foot model provides clinically acceptable measurements of ankle and midfoot angles: a dual fluoroscopy study. *Gait & Posture, 85*, 258–265.

35. De Asla, R. J., Wan, L., Rubash, H. E., & Li, G. (2006). Six dof in vivo kinematics of the ankle joint complex: application of a combined dual-orthogonal fluoroscopic and magnetic resonance imaging technique. *Journal of Orthopaedic Research, 24*, 1019–1027.

36. Koo, S., Lee, K. M., & Cha, Y. J. (2015). Plantar-flexion of the ankle joint complex in terminal stance is initiated by subtalar plantar-flexion: a bi-planar fluoroscopy study. *Gait & Posture, 42*, 424–429.

37. Roach, K. E., Wang, B., Kapron, A. L., Fiorentino, N. M., Saltzman, C. L., Bo Foreman, K., & Anderson, A. E. (2016). In vivo kinematics of the tibiotalar and subtalar joints in asymptomatic subjects: a high-speed dual fluoroscopy study. *Journal of Biomechanical Engineering, 138*, 091006.

38. Phan, C. B., Shin, G., Lee, K. M., & Koo, S. (2019). Skeletal kinematics of the midtarsal joint during walking: Midtarsal joint locking revisited. *Journal of Biomechanics, 95*, 109287.

39. Camp, A. L., & Brainerd, E. L. (2014). Role of axial muscles in powering mouth expansion during suction feeding in largemouth bass (micropterus salmoides). *Journal of Experimental Biology, 217*, 1333–1345.

40. Kambic, R. E., Roberts, T. J., & Gatesy, S. M. (2014). Long-axis rotation: a missing degree of freedom in avian bipedal locomotion. *Journal of Experimental Biology, 217*, 2770–2782.

41. Camp, A. L., Roberts, T. J., & Brainerd, E. L. (2015). Swimming muscles power suction feeding in largemouth bass. *Proceedings of the National Academy of Sciences, 112*, 8690–8695.

42. Kobayashi, T., No, Y., Yoneta, K., Sadakiyo, M., & Gamada, K. (2013). In vivo kinematics of the talocrural and subtalar joints with functional ankle instability during weight-bearing ankle internal rotation: a pilot study. *Foot & Ankle Specialist, 6*, 178–184.

43. Fukano, M., Kuroyanagi, Y., Fukubayashi, T., & Banks, S. (2014). Three-dimensional kinematics of the talocrural and subtalar joints during drop landing. *Journal of Applied Biomechanics, 30*(1), 160–165.

44. Wang, M. C., Geng, X., Wang, S., Ma, M. X., Wang, M. X., Huang, M. J., Zhang, M. C., Chen, M. L., Yang, J., & Wang, K. (2016). In vivo kinematic study of the tarsal joints complex based on fluoroscopic 3d–2d registration technique. *Gait & Posture, 49*, 54–60.

45. Brainerd, E. L., Baier, D. B., Gatesy, S. M., Hedrick, T. L., Metzger, K. A., Gilbert, S. L., & Crisco, J. J. (2010). X-ray reconstruction of moving morphology (xromm): precision, accuracy and applications in comparative biomechanics research. *Journal of Experimental Zoology Part A: Ecological Genetics and Physiology, 313*, 262–279.

46. Knörlein, B. J., Baier, D. B., Gatesy, S. M., Laurence-Chasen, J., & Brainerd, E. L. (2016). Validation of xmalab software for marker-based xromm. *Journal of Experimental Biology, 219*, 3701–3711.

47. Miranda, D. L., Schwartz, J. B., Loomis, A. C., Brainerd, E. L., Fleming, B. C., & Crisco, J. J. (2011). Static and dynamic error of a biplanar videoradiography system using marker-based and markerless tracking techniques. *Journal of Biomechanical Engineering-Transactions of the Asme, 133*, 121002.

48. Cross, J. A., Mchenry, B. D., Molthen, R., Exten, E., Schmidt, T. G., & Harris, G. F. (2017). Biplane fluoroscopy for hindfoot motion analysis during gait: A model-based evaluation. *Medical Engineering & Physics, 43*, 118–123.

49. Kessler, S. E., Rainbow, M. J., Lichtwark, G. A., Cresswell, A. G., D'andrea, S. E., Konow, N., & Kelly, L. A. (2019). A direct comparison of biplanar videoradiography and optical motion capture for foot and ankle kinematics. *Frontiers in Bioengineering and Biotechnology, 7*, 199.

50. Maharaj, J. N., Kessler, S., Rainbow, M. J., D'andrea, S. E., Konow, N., Kelly, L. A., & Lichtwark, G. A. (2020). The reliability of foot and ankle bone and joint kinematics measured with biplanar videoradiography and manual scientific rotoscoping. *Frontiers in Bioengineering and Biotechnology, 8*, 106.

51. Caputo, A. M., Lee, J. Y., Spritzer, C. E., Easley, M. E., Deorio, J. K., Nunley, J. A., & Defrate, L. E. (2009). In vivo kinematics of the tibiotalar joint after lateral ankle instability. *The American Journal of Sports Medicine, 37*, 2241–2248.

52. Peltz, C. D., Haladik, J. A., Hoffman, S. E., Mcdonald, M., Ramo, N. L., Divine, G., Nurse, M., & Bey, M. J. (2014). Effects of footwear on three-dimensional tibiotalar and subtalar joint motion during running. *Journal of Biomechanics, 47*, 2647–2653.